JACS
JOURNAL OF THE AMERICAN CHEMICAL SOCIETY
Article
pubs.acs.org/JACS

Improving Paclitaxel Delivery: *In Vitro* and *In Vivo* Characterization of PEGylated Polyphosphoester-Based Nanocarriers

Fuwu Zhang,[†] Shiyi Zhang,[†] Stephanie F. Pollack,[†,‡] Richen Li,[†] Amelia M. Gonzalez,[†] Jingwei Fan,[†] Jiong Zou,[†] Sarah E. Leininger,[†] Adriana Pavía-Sanders,[†] Rachel Johnson,[§] Laura D. Nelson,[⊥] Jeffery E. Raymond,[†,‡] Mahmoud Elsabahy,[†,‡,∥] Dennis M. P. Hughes,[⊥] Mark W. Lenox,[§] Tiffany P. Gustafson,*[,†,‡] and Karen L. Wooley*[,†,‡]

[†]Departments of Chemistry, Chemical Engineering, and Materials Science and Engineering, [‡]Laboratory for Synthetic-Biologic Interactions, and [§]Texas A&M Institute for Preclinical Studies, Texas A&M University, College Station, Texas 77842, United States

[∥]Department of Pharmaceutics, and Assiut International Center of Nanomedicine, Al-Rajhy Liver Hospital, Assiut University, 71515 Assiut, Egypt

[⊥]Department of Pediatric Research, The University of Texas MD Anderson Cancer Center, Houston, Texas 77030, United States

Supporting Information

ABSTRACT: Nanomaterials have great potential to offer effective treatment against devastating diseases by providing sustained release of high concentrations of therapeutic agents locally, especially when the route of administration allows for direct access to the diseased tissues. Biodegradable polyphosphoester-based polymeric micelles and shell cross-linked knedel-like nanoparticles (SCKs) have been designed from amphiphilic block-graft terpolymers, PEBP-*b*-PBYP-*g*-PEG, which effectively incorporate high concentrations of paclitaxel (PTX). Well-dispersed nanoparticles physically loaded with PTX were prepared, exhibiting desirable physiochemical characteristics. Encapsulation of 10 wt% PTX, into either micelles or SCKs, allowed for aqueous suspension of PTX at concentrations up to 4.8 mg/mL, as compared to <2.0 μg/mL for the aqueous solubility of the drug alone. Drug release studies indicated that PTX released from these nanostructures was defined through a structure−function relationship, whereby the half-life of sustained PTX release was doubled through cross-linking of the micellar structure to form SCKs. *In vitro*, physically loaded micellar and SCK nanotherapeutics demonstrated IC_{50} values against osteosarcoma cell lines, known to metastasize to the lungs (CCH-OS-O and SJSA), similar to the pharmaceutical Taxol formulation. Evaluation of these materials *in vivo* has provided an understanding of the effects of nanoparticle structure−function relationships on intratracheal delivery and related biodistribution and pharmacokinetics. Overall, we have demonstrated the potential of these novel nanotherapeutics toward future sustained release treatments via administration directly to the sites of lung metastases of osteosarcoma.

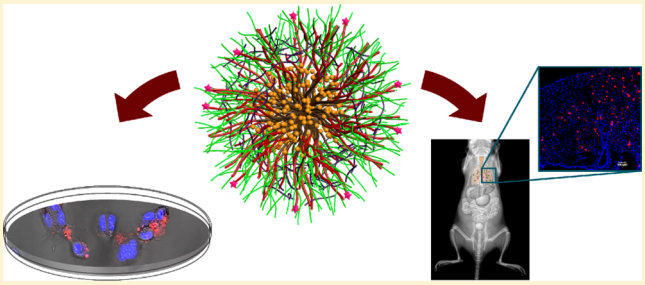

INTRODUCTION

Nanomedicines have great potential to provide effective treatment against devastating diseases by providing sustained release of significant quantities of therapeutic agents locally, especially when the route of administration allows for direct access to the diseased tissues. Our interest focuses on the design of polymer-based nanotherapeutics toward the treatment of osteosarcoma lung metastases. Osteosarcoma is the most common primary cancer of bone in children and adolescents, with a peak incidence in adolescence (age range <5 to ∼40 years), no proven etiology, and a high fatality rate (70% survival at 5 years for nonmetastatic patients, and <30% for those presenting with metastasis).[1,2] The most common site of metastasis is the lung, followed by other bones, with approximately 40% of patients presenting with overt metastasis, and 90% estimated to have micrometastatic disease at diagnosis.[3,4] Osteosarcoma is treated with combination chemotherapy (believed essential to eliminate micrometastatic disease) and complete surgical excision of the primary tumor (either amputation or limb salvage).[5,6] Once micrometastases grow into recurrent, overt disease, tumors are often resistant to conventional chemotherapy, and unresectable recurrent disease is uniformly fatal.[5,7]

It has been demonstrated that drugs delivered to the respiratory tract in liposomal formulation resulted in high pulmonary drug concentration, reduced systemic toxicity, and reduced dosage requirements compared with parenteral and oral administration.[8−10] Standard delivery formulations for paclitaxel (PTX) are generally administered intravenously, resulting in rapid elimination of PTX and multiple undesirable side effects.[11] Further, the poor solubility of this drug, together

Received: December 11, 2014
Published: January 28, 2015

DOI: 10.1021/ja512616s
J. Am. Chem. Soc. 2015, 137, 2056−2066

with the need to dissolve it in toxic carriers prior to delivery, limits the ability to deliver maximally effective doses to patients. To improve efficacy while minimizing systemic toxicity and harmful side effects, it has been suggested that targeting of PTX to the site of disease via aerosol-based delivery would be desirable, and may hold great potential. Unfortunately, the unmodified drug's solubility and overall stability at the high concentrations necessary for such administration remain hurdles to the success of such delivery methods.[12] Our hypothesis is that local inhalation-based delivery of high quantities of the chemotherapeutic agent PTX will be effective in the treatment of lung tumors, with degradable polymer-based nanoparticles being able to overcome key challenges of packaging and transport of sufficient drug quantities directly to the site of the metastatic disease, as well as extravasation of the delivery vehicle from the lungs and secondary organs. Therefore, this study is a first step toward the development of a PTX formulation containing high PTX concentrations within well-defined, degradable nanoparticles for the treatment of lung metastasis of osteosarcoma and other cancers that occur in the lung.

PTX, a mitotic inhibitor originally isolated from the bark of the Pacific yew *Taxus brevifolia*, is a potent chemotherapeutic agent for the treatment of a variety of cancers, including ovarian, breast, and lung cancers.[13,14] Due to its poor solubility in aqueous solutions, PTX is currently formulated with 1:1 blend of Cremophor EL (polyoxyethylated castor oil) and ethanol, under the trademark of Taxol.[15] However, the intrinsic toxicity of Cremophor EL has caused serious side effects, such as hypersensitivity reactions, nephrotoxicity, neurotoxicity, and myelosuppression.[13,16−18] To avoid these side effects, alternative formulations[19−21] are under development to improve PTX's water solubility and biocompatibility, including Cremophor-free, albumin-bound PTX (Abraxane, PTX water solubility = 5 mg/mL) as a protein−drug suspension.[19,22−24] Taking advantage of the natural tumor uptake of nanosized albumin in the human body, Abraxane has demonstrated increased antitumor activity and reduced toxicity, relative to Taxol.[19,22] Although the packaging of PTX within a prevalent natural protein is an attractive strategy, there are questions as to how to achieve high drug loading without alteration of the protein while maintaining control over protein assembly.[19] Alternatively, synthetic nanoparticles have the potential for greater control over their compositions, structures, and properties, while also allowing for selective domains into which the drug molecules can be packaged.[25]

Recently, an increasing number of polymeric nanoscopic platforms, including polymeric micelles,[20,26] dendrimers,[27] nanogels,[28] brush polymers,[29,30] and liposomes,[8,9,31] have been developed for the delivery of PTX and other chemotherapeutics.[32−34] In particular, polymeric micelles have been rigorously investigated due to their characteristic core−shell morphology, where the hydrophobic cores are utilized for incorporation of hydrophobic drugs (herein PTX) while the hydrophilic shells provide water solubility and prolonged systemic circulation.[25,35,36] For example, NK105 is a micellar nanoparticle formulation currently in clinical trials, where PTX is incorporated in the core of polymeric micelles constructed from an amphiphilic block copolymer comprised of poly(ethylene glycol) (PEG) and polyaspartate segments.[20,37] By utilizing the enhanced permeability and retention (EPR) effect, NK105 demonstrated improved efficacy with reduced toxicity.[37−39] However, dissociation of polymeric micelles upon administration *in vivo* may cause premature release of therapeutics, with loss in the control of delivery.[25,40−42]

To overcome micellar dissociation, shell cross-linking is of significant importance to enhance structural stability, as well as to mediate stimuli-responsive drug release.[25,43] We have previously demonstrated that shell cross-linked knedel-like nanoparticles (SCKs) display improved structural stability while retaining the tunability of size, shape, and surface properties.[25,44,45] Recently, we have demonstrated that PTX could be loaded into the hydrophobic cores of SCKs, increasing the water solubility of PTX while maintaining cytotoxicities comparable to those of free PTX against several cancer cell lines.[46] However, these initial nanotherapeutics suffered from relatively low drug loading percentages, and their solubility limits led to fairly low overall PTX concentrations (<30 μg/mL), making them undesirable for clinical applications. To improve upon these systems, we aimed to design biocompatible and fully degradable drug delivery carriers capable of effective incorporation of PTX at high concentrations in water. Such systems are of high interest due to their increased potential to effectively deliver chemotherapeutics and to be cleared from biological systems via intrinsically built-in degradation pathways.[47]

Polyphosphoesters have been receiving attention due to their biocompatibility, biodegradability, and structural similarity to naturally occurring biomacromolecules, such as DNA and RNA.[47−51] Since the phosphorus atom is pentavalent, reactive pendant groups, including hydroxyl, carboxyl, and alkynyl, may be introduced as side-chain functionalities, allowing polyphosphoesters to be structurally versatile.[47,52,53] Recently, researchers in our laboratory developed a hydrophobic-functional AB diblock copolymer via rapid sequential organocatalyzed ring-opening polymerizations of hydrophobic alkyl- and reactive alkynyl-functionalized cyclic phosphotriesters monomers in a stepwise one-pot manner.[52] By taking advantage of radical-mediated thiol−yne reactions on the clickable alkynyl groups of the B block, this diblock copolymer could be transformed into a variety of amphiphilic block copolymers and assembled into functional nanoparticles tailored for biomedical applications.[52] In this study, we made use of this structurally versatile platform to develop a drug carrier via copper(I)-catalyzed azide−alkyne cycloaddition (CuAAC) for transformation to an amphiphilic labeled polymer, capable of supramolecular assembly into PTX-loaded nanoparticles. Our results demonstrate that these new nanotherapeutic delivery vehicles show potential toward future sustained release treatments via administration directly to the site of lung metastasis of osteosarcoma, whereby shell cross-linking reduced the rate of drug release and increased the lung retention time.

■ RESULTS AND DISCUSSION

In order to construct high-capacity and scalable polymer-based nanotherapeutics, we designed supramolecular and covalently stabilized nanoparticles, formed from biocompatible, degradable, and structurally versatile amphiphilic block terpolymers that were prepared by efficient "click-type" chemistries, including rapid ring-opening polymerizations (ROPs) and azide−alkyne Huisgen cycloaddition reactions (Figure 1). The block copolymer consists of a degradable and water-soluble polyphosphoester backbone, for which the first block contains alkyl side chains for creating a hydrophobic environment and the second block is comprised of alkynyl side chains

DOI: 10.1021/ja512616s
J. Am. Chem. Soc. 2015, 137, 2056−2066

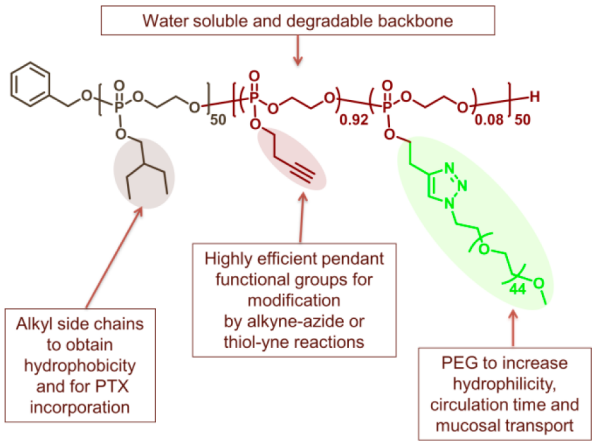

Figure 1. Design of the amphiphilic block terpolymer for therapeutic delivery.

for post-polymerization modifications. The alkynes in the second block were used to graft PEG chains onto the block copolymer through CuAAC, to increase the polymer hydrophilicity, and also for the conjugation of near-infrared fluorescent dyes (IRDye 800CW), to facilitate imaging *in vivo* and determination of particle pharmacokinetics (PK).

The amphiphilic nature of the resulting copolymers allowed for the formation of micelles in aqueous solution, which are capable of encapsulating PTX through hydrophobic interactions within the core. Crucial to biomedical applications is that PEG is a well-known and non- to minimally toxic coating for nanoparticles that imparts "stealth" effects. PEGylation often results in minimal protein adsorption and mononuclear phagocyte system (MPS) clearance, and leads to prolonged blood circulation times and an increase in mucosal transport.[25,54−59] Mucosal transport, in particular, is key to the development of inhalation-based chemotherapeutics in the treatment of lung metastasis of osteosarcoma. Important for tailoring this platform is the presence of remaining unreacted alkynes, which were utilized for post-graft cross-linking and could be adapted for further modification.

Synthesis of PEBP-*b*-PBYP-*g*-PEG. The amphiphilic block terpolymer PEBP-*b*-PBYP-*g*-PEG was synthesized utilizing click-type chemistries, which are attractive as they occur rapidly and involve (nearly) quantitative conversions of reagents, high functional group tolerance, and minimal side reactions (Scheme 1A). A hydrophobic-functional AB diblock polyphosphoester was synthesized via sequential ROPs, a well-established approach to synthesize degradable polymers such as polyesters,[54,60,61] polypeptides,[62,63] polycarbonates,[64−66] and polyphosphoesters.[52,53,67] Briefly, the diblock copolymer poly(2-ethylbutoxy phospholane)-*block*-poly(2-butynyl phospholane) (PEBP-*b*-PBYP) was synthesized via sequential ROPs of 2-ethylbutoxy phospholane (EBP) and 2-butynyl phospholane (BYP), catalyzed by organocatalyst 1,5,7-triazabicyclo[4.4.0]-dec-5-ene (TBD) at 0 °C and −10 °C, respectively, in dichloromethane, with benzyl alcohol as an initiator (Scheme 1A). Phosphorus-31 nuclear magnetic resonance (^{31}P NMR) spectroscopy was used to monitor monomer conversion. It was found that over 99% conversion was reached after 3 min for the alkyl monomer, while the second alkyne monomer required less than 3 min to reach 99% conversion, even at lower monomer concentration and temperature. The reaction was quenched by the addition of acetic acid, and purified by precipitation from dichloromethane into pentane and diethyl ether (3:1) mixture, followed by centrifugation. Gel permeation chromatographic (GPC) analysis showed that both PEBP and PEBP-*b*-PBYP exhibited monomodal molecular weight distributions with relatively low polydispersity indices (PDIs) of 1.14 and 1.24, respectively (Scheme 1B). The decreased retention time of PEBP-*b*-PBYP, relative to PEBP, demonstrated successful chain extension. PEGylation was achieved in *N*,*N*-dimethylformamide (DMF) via CuAAC quantitatively for CH_3O-PEG_{2k}-azido-functionalized PEG grafts, as confirmed by proton NMR (^{1}H NMR) spectroscopy and GPC (Scheme 1). To remove copper ions, the reaction mixture was passed through a neutral alumina column and dialyzed against nanopure water suspended with Chelex for 2 d in a cold room at ca. 4 °C. A white powder-like product was obtained after lyophilization. The residual copper concentration was analyzed by ICP-MS, revealing a mass fraction of less than 10 ppm, which is acceptable for drug delivery applications.

Evaluation of PEBP-*b*-PBYP-*g*-PEG Micelles and SCKs as PTX Delivery Vehicles. With an average of only four PEG grafts per polyphosphoester block terpolymer backbone, PEBP-*b*-PBYP-*g*-PEG was found to be highly water-soluble, and PTX-loaded micelles and SCKs could be prepared in a facile manner

Scheme 1. (A) Synthesis of PEBP-*b*-PBYP-*g*-PEG via Sequential Ring-Opening Polymerization of EBP and BYP, Followed by PEGylation via CuAAC, and (B) GPC Traces of PEBP Homopolymer, PEBP-*b*-PBYP Diblock Copolymer, and PEBP-*b*-PBYP-*g*-PEG Terpolymer

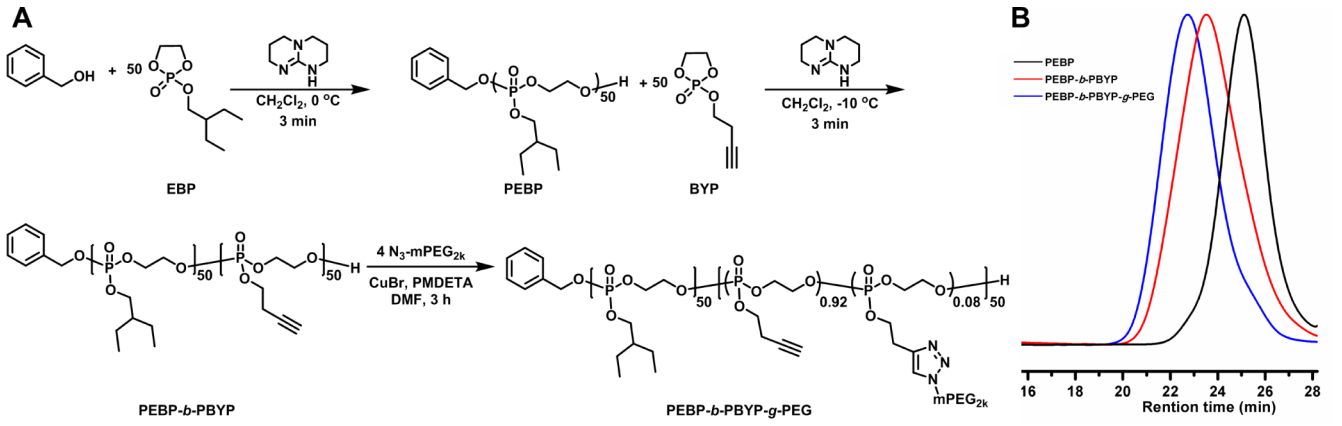

DOI: 10.1021/ja512616s
J. Am. Chem. Soc. 2015, 137, 2056−2066

(Figure 2). PTX-loaded micelles were formed by dissolving the polymer and PTX in ethanol, followed by the removal of

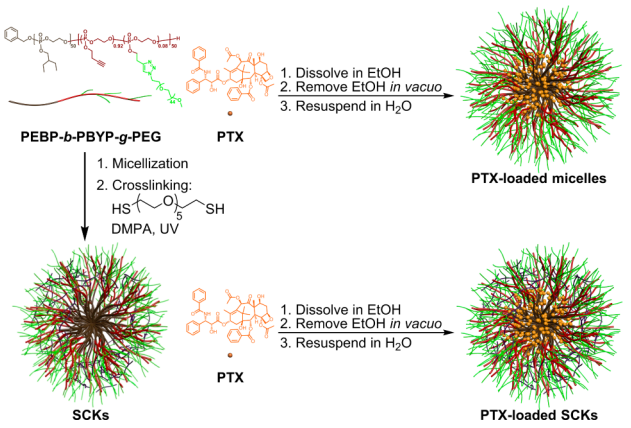

Figure 2. Schematic representation of the formation of micelles and SCKs physically loaded with PTX.

ethanol *in vacuo* and resuspension in nanopure water, with 5 min sonication to allow for the formation of well-dispersed micelles.

The SCKs were prepared by supramolecular assembly of PEBP-*b*-PBYP-*g*-PEG into micelles, followed by shell cross-linking via thiol−yne click chemistry. The block graft terpolymer was first dissolved in methanol; subsequent addition of water directed the hydrophobic PEBP segments to aggregate and form the core domains of the micelles, while the hydrophilic PEG formed the shell domains. The formed micelles were then shell cross-linked with hexa(ethylene glycol) dithiol (0.2 equiv to alkyne groups) in the presence of 2,2-dimethoxy-2-phenylacetophenone (DMPA) and UV irradiation at 365 nm. The resulting SCKs were dialyzed for 2 d to remove organic solvent and other small molecules and subsequently lyophilized to yield a yellowish powder. Upon dissolution in ethanol, the SCK suspension displayed strong light scattering when a laser light was passed through the solution, indicating successful cross-linking, with a number-averaged diameter of ca. 33 nm as measured by dynamic light scattering (DLS) (Supporting Information, Figure S1). PTX was loaded into SCKs utilizing the procedure for the PTX-loaded micelles, using SCKs in place of the polymer PEBP-*b*-PBYP-*g*-PEG (Figure 2). Importantly, long-term storage (>6 months) of lyophilized PTX-loaded micelles and SCKs did not affect their properties upon resuspension in aqueous solution.

The PTX concentration and loading capacity were optimized, for both the micelles and SCKs, by tuning PTX loading percentages and polymer or SCK concentrations (Supporting Information, Table S1). The actual PTX concentrations were determined by HPLC at a flow rate of 1 mL/min using a mixture of CH_3CN and 20 mM aqueous NH_4OAc at a ratio of 45:55 as the eluent. At 10 wt% loading, the PTX concentrations increased from 1.0 mg/mL to 4.8 mg/mL with increasing polymer concentration for both micelles and SCKs (Table S1, entries 1−4 and 7−9, respectively). These nanoparticles were visually stable in nanopure water, without any precipitation and could be stored for more than 1 month at 4 °C. However, when the loading percentage increased to 15 or 20 wt% (Table S1, entries 5 and 6, respectively), the obtained nanoparticles were only stable in nanopure water for ca. 2 d, at which time significant quantities of white precipitates were visualized. Incorporation of PTX into micelles or SCKs appeared to be highly effective, as all initially added PTX was visibly dispersed within the transparent particle solutions at high concentrations of 10 wt% (entry 4 for micelles, entry 9 for SCKs). At such concentrations, both micelles and SCKs demonstrated homogeneous light scattering when a red laser was passed through the solutions, suggesting that well-dispersed nanoparticles encapsulating PTX were prepared (Supporting Information, Figure S2). Compared with our previous SCK formulations, the PTX concentration in aqueous solution achieved in this study was increased approximately 160 times to 4.8 mg/mL, which is equal to benchmarking systems such as Abraxane and NK105, as well as many of the high loading polymeric micellar delivery systems reported in the literature.[20,26,60,68]

The sizes of the micelles and SCKs physically loaded with PTX were characterized both by DLS and transmission electron microscopy (TEM). DLS analysis indicated that the number-averaged hydrodynamic diameters ($D_{h(number)}$) of the particles were 14 ± 4 and 24 ± 6 nm (Figure 3A,D), respectively, with

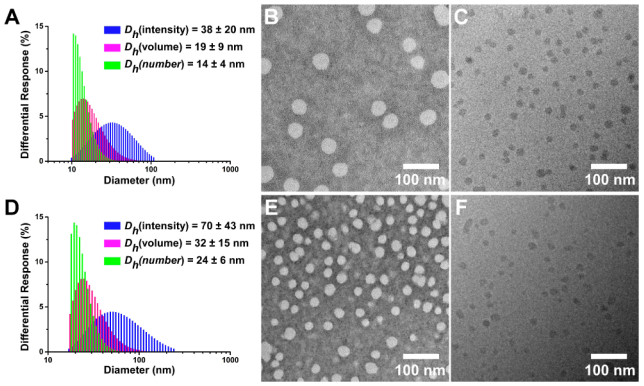

Figure 3. Characterization of nanoparticle sizes for PTX-loaded micelles (A−C) and SCKs (D−F). Displayed from left to right respectively: DLS histograms displaying their hydrodynamic diameters in nanopure water, TEM sample negatively stained by uranyl acetate, and cryo-TEM images without staining.

negative zeta potentials of −40 mV. TEM images demonstrated that both micelles and SCKs were well dispersed and had relatively uniform dry-state substrate-adsorbed diameters of ca. 42 ± 5 and 24 ± 4 nm, respectively (Figure 3B,E). As PPEs are soft materials (T_g = −51 °C), the micellar structures could not maintain their spherical shapes in the dry state on TEM grids, tending to become flattened, leading to an observed diameter larger than their D_h. Cross-linking to create SCKs limited the extent of deformation of the nanostructures. In an effort to more accurately determine the dry state diameters, cryo-TEM measurements were performed on both PTX-loaded micelles and SCKs, where specimens were prepared in vitreous ice to view the unaltered macromolecular co-assembly, without shape deformation or staining perturbation (Figure 3C,F). It was confirmed that both micelles and SCKs had diameters of ca. 17 nm with narrow size distributions, which was in agreement with data obtained from DLS measurements.

The release of PTX from micelles or SCKs was evaluated by monitoring the decreasing concentration of PTX from a solution of loaded micelles or SCKs dialyzed (MWCO 10 kDa) against PBS at 37 °C over 3 d (Figure 4). It was found that both micelles and SCKs released PTX at a slow and sustained

DOI: 10.1021/ja512616s
J. Am. Chem. Soc. 2015, 137, 2056−2066

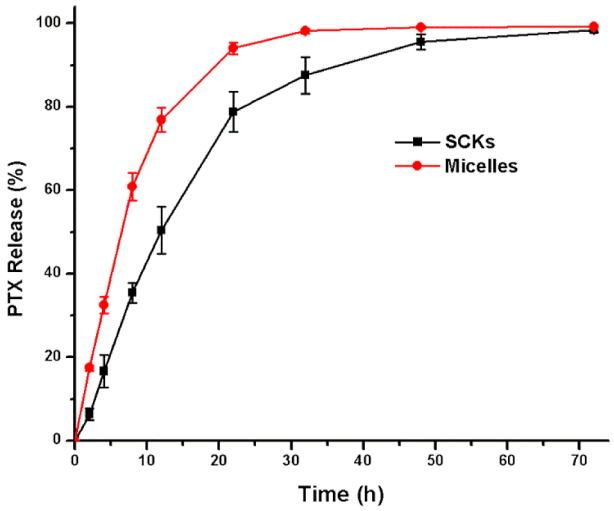

Figure 4. Release of paclitaxel that was loaded into either micelles or SCKs and studied by a dialysis method over 3 d at 37 °C in PBS, measured in triplicate.

rate. As expected, shell cross-linking created an additional physicochemical layer that retarded drug transport through the shell, providing a decreased rate of release for PTX from SCKs, as compared to the corresponding micelle precursors. The apparent PTX release half-life ($t_{1/2}$) from micelles and SCKs were determined to be 6.5 and 12 h, respectively. Therefore, the release profiles can be potentially tuned simply by altering the degree of cross-linking.[43]

The *in vitro* hydrolytic degradation of the PEBP-*b*-PBYP-*g*-PEG micelles was evaluated at different pH values utilizing ^{31}P NMR spectroscopy to monitor the cleavage of their phosphodiester backbones and phosphoester side chains (Supporting Information, Figure S5).[69,70] At neutral pH 7.4, the nanoparticles displayed high stability, observing only a small degradation peak (<10%) at 0.35 ppm by ^{31}P NMR after incubation in PBS for 103 d (Figure S5A). Generally, it has been shown that the hydrolytic degradation rate is greatly influenced by side-chain functionalities; for example, amino group-containing cationic nanoparticles degraded much faster compared to anionic, nonionic, and zwitterionic nanoparticles.[70−74] We hypothesize that the increased stability of PEBP-*b*-PBYP-*g*-PEG arises from not only a lack of nucleophiles in the neutral PBS but also the densely packed $mPEG_{2k}$ grafted surface, which leads to limited exposure of the polymer to nucleophiles within the surrounding environment. As expected, the extent of hydrolysis increased significantly under both acidic (pH 1, Figure S5B) and basic conditions (pH 10, Figure S5C).[69] For example, at pH 10, the ^{31}P NMR signal from PBYP decreased by more than 70% after 115 d.

Near-Infrared Labeling of PEBP-*b*-PBYP-*g*-PEG Micelles and SCKs. To investigate the *in vitro* cellular uptake and *in vivo* biodistribution and PK of the PEBP-*b*-PBYP-*g*-PEG micelles and SCKs, a hydrophilic near-infrared (NIR) fluorescent dye, IR800CW azide, was grafted to the polymer via CuAAC in nanopure water (Supporting Information, Figure S3). The unreacted dye was removed using a Sephadex G-25 column followed by dialysis for 2 d (MWCO 12−14 kDa). Removal of the unconjugated IR800CW dye was confirmed by the disappearance of the free dye peak in DMF GPC (Supporting Information, Figure S4). Confirmation of covalent dye conjugation for the purified polymer−dye conjugate was also examined by fluorescence spectroscopy. As previously reported for PPE block copolymers, the PPE is capable of undergoing degradation during gel electrophoresis; thus, alternative spectroscopic techniques (fluorescence anisotropy (r) and intensity-averaged fluorescence lifetime (τ_i)) were utilized to confirm successful conjugation (Supporting Information, Table S2).[75]

The use of spectroscopic techniques to evaluate dye−nanoparticle conjugation is advantageous, as the results can provide valuable information on the dynamic behavior of the fluorophores within their supramolecular and external environments.[75] In the case of evaluating dye−macromolecule conjugation of NIR cyanine dyes, such as IR800CW, the use of r and τ_i measurements is often considered difficult. The trouble with measuring changes in these spectroscopic properties following conjugation of NIR dyes lies with their short fluorescence lifetimes in aqueous solvents (<1.0 ns), traditionally elongated structures that lead to high r measurements for the unconjugated dyes (>0.2) and reliance upon extended linkers utilized for conjugation resulting in higher local mobility or "wobbling" of NIR dyes upon coupling.[76] Therefore, when utilizing such techniques, small changes that may not be considered of interest in the case of longer-lived and more compact visible-emitting dyes take on increased significance when evaluating conjugation of NIR cyanine-based dyes.

Following grafting of the dye IR800CW to PEBP-*b*-PBYP-*g*-PEG micelles and SCKs, both r and τ_i, were evaluated, and changes in both spectroscopic properties were observed (Table S2). The r and τ_i of both the free dye and physical mixtures of the free dye with polymeric nanomaterials resulted in starting anisotropy values ca. 0.220 and τ_i near 0.500 ns. Upon grafting of the dye to both micelles and SCKs, statistically significant increases in r and τ_i were observed in both water and pH 7.4 PBS, indicating that the dye was covalently attached to, rather than physically associated with, the polymeric nanomaterials.

Table 1. Comparison of the IC_{50} Values of PTX (as a Taxol-Mimicking Formulation), Physically Loaded PTX Micelles (with and without the NIR Label IR800CW), and SCKs in Both Control (OVCAR-3) and Osteosarcoma (CCH-OS-O and SJSA) Cell Lines

	IC_{50} (μM)			
formulation	OVCAR-3	RAW 264.7	CCH-OS-O	SJSA
Taxol[a]	0.005 ± 0.002	0.040 ± 0.010	0.019 ± 0.001	0.047 ± 0.006
PTX micelles	0.015 ± 0.010	0.100 ± 0.040	0.028 ± 0.001	
IR800CW PTX micelles	0.016 ± 0.009		0.028 ± 0.001	0.068 ± 0.007
PTX SCKs	0.010 ± 0.008	0.080 ± 0.020	0.014 ± 0.001	

[a]Taxol-mimicking formulation: Cremophor-EL and ethanol, 1:1 v/v.

DOI: 10.1021/ja512616s
J. Am. Chem. Soc. 2015, 137, 2056−2066

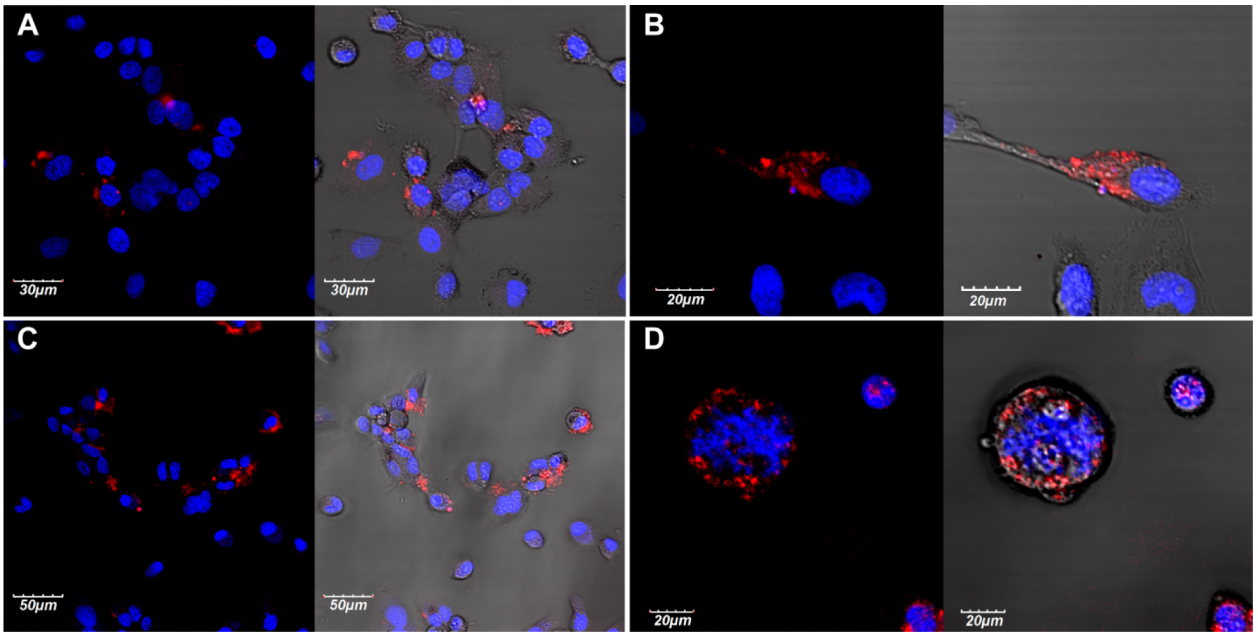

Figure 5. Confocal microscopy images demonstrating cellular internalization of both unloaded micelles (A,B) and micelles physically loaded with PTX (C,D) into CCH-OS-O cells (A, magnification = 60×, scale bars = 30 μm; C, magnification = 40×, scale bars = 50 μm; B and D, magnification = 100×, scale bars = 20 μm; blue = DAPI (nuclear stain) and red = IR800CW from NIR labeled micelles). Images to the right overlay fluorescence on the DIC.

By utilizing both aqueous solvents (water and PBS), the effect of cross-linking on the ability of the polymeric materials to interact with the surrounding solvated environment could be probed. In this case, the SCK displayed no change in either the r or τ_i measurements, while the micellar particles displayed small changes that are not statistically different. Given the noted nature of such measurements with NIR cyanine dyes, these changes cannot be entirely discounted to lack meaning, but rather may be considered indicative that cross-linking does have an effect upon the ability of these polymeric materials to freely interact with their surrounding environment, which is also supported by previous findings.[25,43,45]

Nanoparticle Toxicity and Cellular Uptake. The *in vitro* cytotoxic effects of the physically PTX-loaded micelles and SCKs were measured against human ovarian adenocarcinoma cells (OVCAR-3), RAW 264.7 mouse macrophages (RAW 264.7), CCH-OS-O, and SJSA cell lines to establish their IC_{50} values at 72 h incubation time, as compared to that of PTX (as a Taxol-mimicking formulation; Cremophor-EL and ethanol, 1:1 v/v) (Table 1). OVCAR-3 cells serve as a control for comparability to previously studied polymeric chemotherapeutic delivery vehicles,[20,68,77] while the osteosarcoma cell lines CCH-OS-O and SJSA demonstrate the effective toxicity of the PTX-loaded materials toward the targeted disease, lung metastasis of osteosarcoma. Polymeric micelles and SCKs physically loaded with 10 wt% PTX displayed *in vitro* cytotoxicities comparable to those of the Taxol-mimicking formulation. Despite the slower PTX release, PTX-loaded SCKs exhibited only slightly higher cytotoxicity compared to PTX-loaded micelles. As a result of their greater sensitivity to PTX, the difference was more significant on OVCAR-3 cells, in comparison to the other cell lines. The reduced cytotoxic effects of these nanoscopic carriers may be, in part, due to the fast release of lipophilic PTX from the small molecular Cremophor-EL surfactants, which can diffuse passively through cell membranes and cause cytotoxicity. Grafting of IR800CW to the micellar polymer structures had no effect on nanoparticle cytotoxicity in OVCAR-3 or CCH-OS-O cell lines and, thus, is not expected to change the outcomes in RAW 264.7 and SJSA cell lines or as regards the cytotoxicity of the SCKs. As a control, the cytotoxicity of the corresponding nanoparticles without PTX was evaluated, and they were found to be nontoxic at the tested concentrations.

After it was established that the IC_{50} values for the PTX-loaded micelles and SCKs in osteosarcoma cell lines were comparable to the pharmaceutical Taxol-mimicking formulation, a cell uptake study by confocal microscopy was conducted, using CCH-OS-O osteosarcoma cells. The resulting images support cellular internalization of both the micellar (Figure 5) and SCK (Supporting Information, Figure S6) nanostructures, whereby nuclear degradation appeared to occur, presumably, upon PTX release within the cellular environment following internalization of PTX-loaded nanoparticles (Figure 5C,D, micelles). When the unloaded micelles and SCKs were taken up by the CCH-OS-O cells (Figure 5A,B, micelles), there appeared to be no effect, which reflected the reported lack of cytotoxicity. These studies further demonstrate the cytotoxicity of these PTX-loaded materials and highlight their ability to deliver PTX and effectively disrupt the growth of osteosarcoma cells.

Biodistribution and Pharmacokinetics. Previous research utilizing liposomal[8−10] and nanoparticle[78,79] drug formulations has demonstrated that drugs delivered directly to the respiratory tract can result in high pulmonary drug concentration, reduced systemic toxicity, and reduced dosage requirements vs parenteral or oral administration.[8−10] Additionally, these studies revealed that delivery of therapeutics by inhalation-based methods shows great promise toward increased efficacy of treatment, relative to systemic delivery. However, unlike in the case of systemic delivery, these studies have largely avoided evaluating the overall behavior of the nanoparticles themselves as regards lung extravasation and

DOI: 10.1021/ja512616s
J. Am. Chem. Soc. 2015, 137, 2056−2066

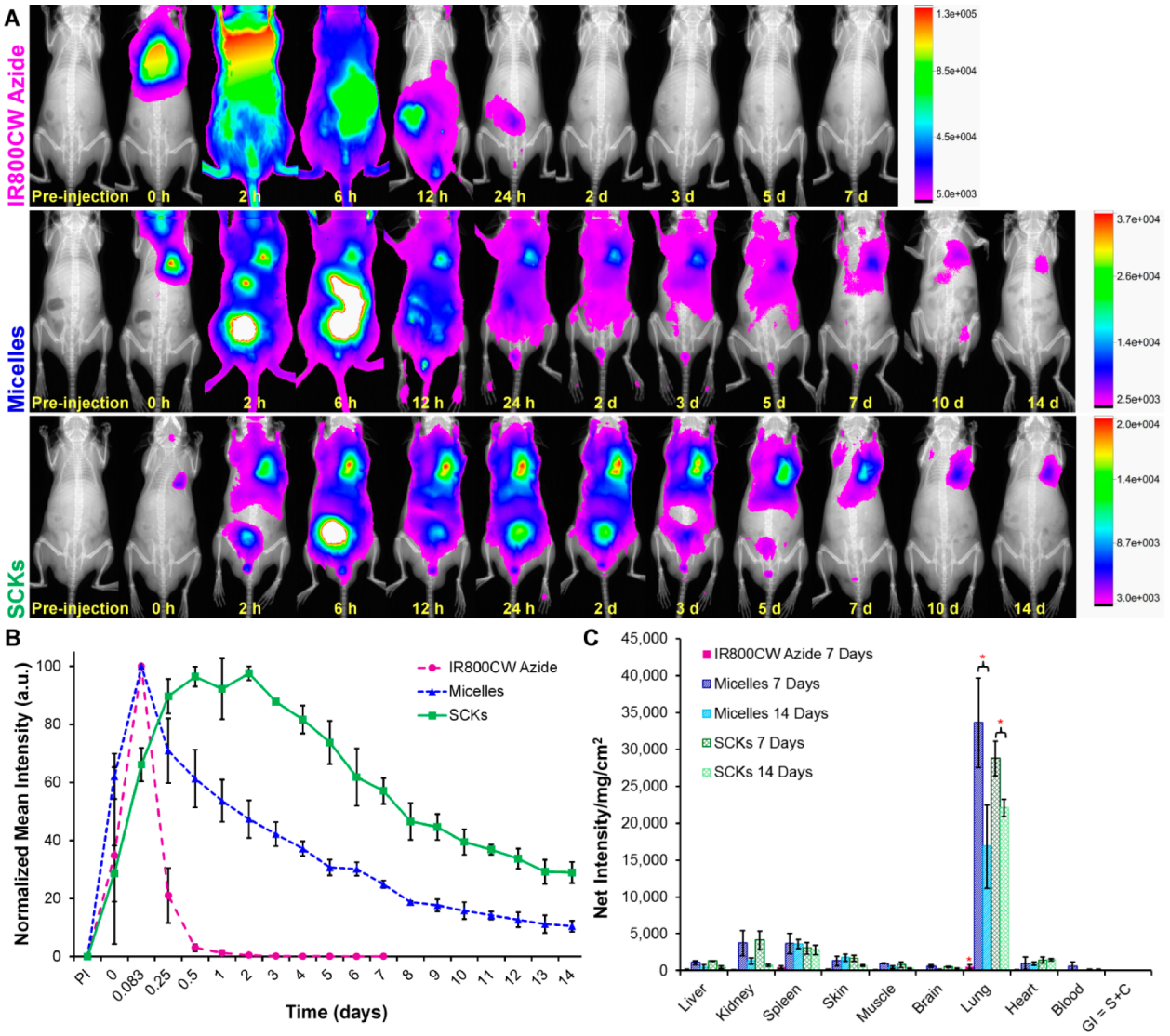

Figure 6. (A) Overlaid optical on X-ray images of the small-molecule dye IR800CW Azide (top) vs PEBP-*b*-PBYP-*g*-PEG-*g*-IR800CW micelles (middle) and SCKs (bottom) collected as a function of time. (B) PK profiles of normalized mean fluorescence intensity as a function of time for the free dye (IR800CW azide) and IR800CW-labeled micelles and SCKs. (C) Quantified biodistribution data collected *ex vivo* on harvested organs at 7 and 14 d PI for IR800CW azide vs IR800CW-labeled micelles and SCKs.

whole body biodistribution. Studies addressing nanoparticle disposition and biokinetics from aerosol-based treatments have focused on nondegradable and/or inorganic nanoparticles evaluated by *ex vivo* tissue analysis, or concentrated on specific interactions, such as translocation of particles from the lungs to lymph nodes.[10,78−80] While these studies provide valuable information as to nanoparticle location and toxicology, initial screening via optical imaging *in vivo* would allow for monitoring of real time trafficking, from which PK data and routes of excretion can be evaluated. Of significant interest was evaluation of the PK of the degradable PEBP-*b*-PBYP-*g*-PEG micelles and SCKs, and determination of whether cross-linking would affect the rate of extravasation (k_{ex}), with correlation to the *in vitro* findings.

In the case of the PEBP-*b*-PBYP-*g*-PEG micelles and SCKs presented herein, it was hypothesized that the degradable polymer-based nanoparticles themselves would be capable of extravasation from the lungs and secondary organs on a timeline compatible with repeated dosing of PTX, but that the rate of lung extravasation for micelles vs SCKs would be different, due to the increased stability imparted to SCKs through cross-linking. The hypothesis, as regards extravasation of micelles vs SCKs, was supported by previously reported findings where cross-linked SCKs were shown to have higher morphological stability, undergo slower disintegration, and elicit lower immuno-toxicity than their noncross-linked micellar analogues.[72] Nanoparticle PK were indirectly evaluated by NIR optical imaging, following intratracheal administration to ensure that extravasation of the majority of the delivery vehicle largely occurred within the 1−2 week time frame largely considered appropriate for repeated dosing.[81]

IR800CW azide, PEBP-*b*-PBYP-*g*-PEG-*g*-IR800CW micelles, or SCKs (λ_{ex} = 778 nm, λ_{em} = 792 nm) were administered intratracheally to six mice each. All mice were monitored over 7−14 d by whole-body optical imaging on a Bruker Xtreme *in vivo* preclinical imaging system. The biodistribution of each dye/nanoparticle was imaged at regular intervals, directly post injection (PI), at 2, 6, 12, and 24 h PI and then daily until the appropriate end point of either 7 or 14 d PI (n = 3 mice at each end point *per* injected dye/nanoparticle to reach statistical

DOI: 10.1021/ja512616s
J. Am. Chem. Soc. 2015, 137, 2056−2066

significance) (Figure 6A). For all images, normalized fluorescence intensities over the lung region were obtained through image analysis and plotted vs time to generate PK profiles (Figure 6B) for each experimental group (IR800CW azide, micelles, or SCKs). The rate of extravasation from the lungs (k_{ex}) and $t_{1/2}$ were obtained by fitting the PK profile with a nonlinear curve fit (Table 2). At the study end point, tissue and organs were harvested (liver, kidney, spleen, skin, muscle, brain, lung, heart, blood, and the GI tract (stomach, intestines, cecum, etc.)) and imaged *ex vivo* to obtain end point biodistribution data (Figure 6C).

Table 2. Pharmacokinetics of the Dye IR800CW Azide and Its Micellar and SCK Conjugates

agent	latency (d)	k_{ex}[a] (d^{-1})	$t_{1/2}$[b] (d)
IR800CW azide	0.08	9.29	0.16
micelles	0.08	0.17	4.18
SCKs	2.00	0.11	8.28

[a] k_{ex} = rate of extravasation from the lungs [b] $t_{1/2} = t_{1/2}$ + latency

PK analysis established the lung extravasation $t_{1/2}$ for the PEBP-*b*-PBYP-*g*-PEG-*g*-IR800CW micelles to be ca. 4 d (Table 2), whereas the small-molecule NIR probe exhibited a $t_{1/2}$ of 4 h, with >85% cleared from the lungs within 12 h and the entire body within 1−2 d (Figure 6A,B). The micellar $t_{1/2}$ was supported by the imaging results, suggesting that micelles exhibit extended lung retention of >14 d, at which time the $t_{1/2}$ indicates ca. 7−10% of the original micelle dose should remain present. Alternatively, the polymeric SCKs display a $t_{1/2}$ of ca. 8 d, twice that of their micellar counterparts. The difference in extravasation rates is most likely due to a change in the structure−function relationship, whereby cross-linking leads to added structural stability and decreased interactions with the surrounding biological environment, as compared to the micellar structures, supporting the findings of the NIR spectroscopy study above. We hypothesize that the resulting decrease in external interactions with fluids and other biological elements (proteins, enzymes, etc.) would decrease opportunities for externally induced degradation (e.g., enzymatic), resulting in the observed longer $t_{1/2}$. These studies and findings may be complicated by the indirect detection method, whereby the dye is being tracked independent of whether it is bound to the original nanoparticle, disassembled polymer chains, or partial fragments due to cleavage of the dye from the polymer backbone or polymer backbone degradation. However, the significantly faster biological clearance of the small-molecule dye suggests that the micelle and SCK studies were, in fact, measurements predominantly of nanoparticle/polymer clearance rates.

Ex vivo fluorescence imaging of the collected tissue and organs was evaluated to confirm that the nanomaterials remained largely in the lungs, and to identify secondary organ systems that may have accumulated small quantities of nanomaterials or potential degradation products. Semiquantitative analysis (Figure 6C) reveals that the major site of nanoparticle accumulation, for both micelles and SCKs, was in the lungs (the site of administration) at both 7 and 14 d PI. The clearly observed difference between retention of nanoparticle formulations and unconjugated IR800CW azide over 7 d is statistically significant based upon a student's *t* test ($n = 3$), and supports the reported *in vivo* PK studies. Evaluation of both the *in vivo* and *ex vivo* findings suggests that at least two routes of extravasation from the lungs and excretion from the body may have taken place concurrently. *In vivo* studies revealed both early clearance to the bloodstream and through the mucociliary tract, due to repeated coughing up and swallowing of the micelles or SCKs. Over time, extravasation from the lungs via the mucociliary tract was observed to become negligible, as later images revealed accumulation largely within the kidney and liver, indicating the primary route of extravasation was into the blood. *Ex vivo* findings indicated limited accumulation of both nanomaterials in the kidney and liver, demonstrating that both micelles and SCKs were excreted concomitantly via both the renal and hepatobiliary pathways. When considering the degradable nature of these materials, the findings were not unexpected, as degradation byproducts could be of a multitude of sizes (from partly intact polymers or nanoparticle pieces to small molecules) that are capable of undergoing excretion from the body via either pathway, depending on size.[25] Overall, the $t_{1/2}$ and biodistribution results support the ability of both the micelles and SCKs to undergo extravasation from the lungs and whole body excretion within a timeline reasonable for repeated dosing on a weekly or biweekly basis.

Evaluation of Polymer Retention in Mouse Lungs *Ex Vivo*. To confirm that intratracheal delivery did not solely deliver the PEBP-*b*-PBYP-*g*-PEG-*g*-IR800CW micelles and SCKs to the location of deposition within the lungs, but rather that the nanoparticles are capable of distributing throughout the lung tissue, the general location of the particles was evaluated by confocal microscopy on frozen lung sections. The lungs of mice treated with IR800CW micelles and SCKs ($n = 3$ for each particle) were filled with a 50/50 solution of sterile water/OCT, frozen, and sliced at a thickness of 20 μm in a cross-sectional manner from the distal to proximal end, such that both the left and right lobes were included in each section. Fluorescence images of lung sections (Figure 7 and Supporting Information, Figure S7 display representative images) were obtained after applying mounting media containing DAPI for nuclear staining. NIR signal from IR800CW-labeled nanoparticles was observed throughout both the left and right lobes at distal, medial, and proximal locations for all treated mice, while untreated controls lacked fluorescence signal in the NIR region. Such outcomes indicated that the nanomaterials were capable of migrating from the point of administration throughout the lung, which would be vital in the treatment of widespread metastatic disease.

■ CONCLUSIONS

Polyphosphoester-based amphiphilic block graft terpolymers have been prepared by efficient "click-type" reactions, and were able to undergo coassembly with PTX to form well-defined nanoparticles, as supramolecular micelles and covalently stabilized SCKs. Characterization of the resulting nanotherapeutics demonstrated that they exhibited desirable physiochemical properties when loaded with up to 10 wt% of PTX, a concentration of 4.8 mg/mL in aqueous solution that was a 160-fold increase over our previous SCK formulations.[46] During subsequent drug release studies, it was observed that the $t_{1/2}$ of PTX release for SCKs is nearly double that of their micellar counterparts (12 vs 6.5 h, respectively). These results demonstrated that cross-linking was capable of mediating PTX release by forming an additional physicochemical layer through the shell, the tuning of which could be utilized to further tune the performance of these nanoscopic containers. Residual alkynyl groups along the backbones were modified by attaching

DOI: 10.1021/ja512616s
J. Am. Chem. Soc. 2015, 137, 2056−2066

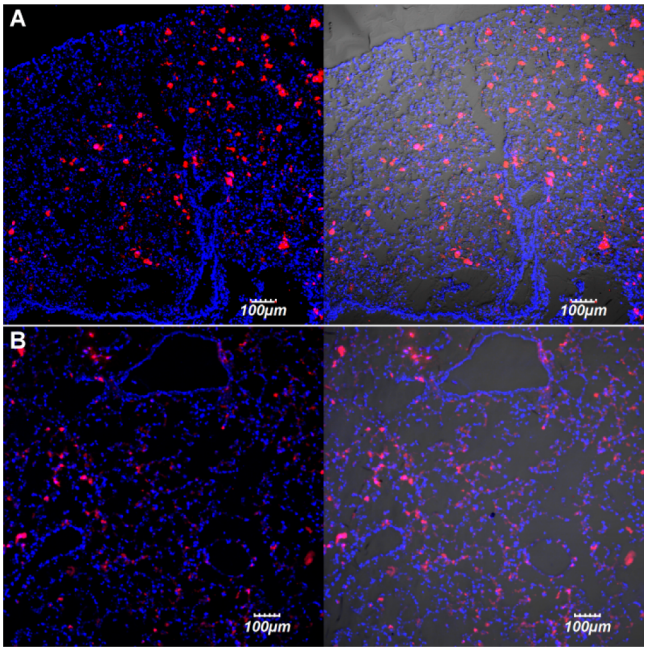

Figure 7. Representative *ex vivo* confocal microscopy *z*-stack of 20 μm lung sections 7 d PI of IR800CW labeled (A) micelles and (B) SCKs (10×, scale bar = 100 μm) supporting distribution of the nanoparticles throughout the lungs of healthy mice (blue = DAPI (nuclear stain) and red = IR800CW NIR labeled nanoparticles). Images to the right overlay fluorescence on the DIC.

the NIR dye IR800CW, enabling their use *in vivo* and *ex vivo* imaging-based studies.

The promising features displayed by these PTX-loaded nanoparticles led to further investigation of their *in vitro* and *in vivo* characteristics to evaluate potential efficacy against known metastatic osteosarcoma cell lines and the potential of the particles toward direct administration to the lung for the treatment of metastatic osteosarcoma tumors. *In vitro*, these micellar formulations had comparable cytotoxicities with the commercially available Taxol-mimicking formulation, further validating them as excellent candidates for translational studies. *In vivo* evaluation of the pharmacokinetics and biodistribution, following intratracheal delivery, revealed that cross-linking has the ability to control the rate of nanoparticle extravasation from the lungs. SCKs were observed to be retained for almost twice the time of their micellar equivalents, ca. 8 d vs Four d, respectively. These extravasation timelines appear to be reasonable for translational development when considering the repeating dosing schedules already in place for PTX chemotherapeutics. Interestingly, we have shown that the structure–function relationship of nanomaterials not only affects *in vitro* outcomes but also has implications on *in vivo* performance and pharmacokinetics following intratracheal delivery to the lungs.

Given the findings presented herein, these new PEBP-*b*-PBYP-*g*-PEG chemotherapeutic delivery vehicles have great potential as nanocarriers, providing sustained release treatments via administration directly to the site of lung metastasis of osteosarcoma. This initial work has established the ability to load drugs into well-designed polymer nanoparticle frameworks, achieve *in vitro* efficacy against relevant cancer cells, and probe the *in vivo* biodistribution of the nonloaded nanoparticles in healthy animals to understand their trafficking behaviors. Important for tailoring this platform is the presence of remaining unreacted alkynes, which could be adapted for further modification, such as attachment of targeting ligands and grafting of imaging agents to evaluate biodistribution and nanoparticle location within tissues. However, key issues remain to be investigated, including the relationships between *in vitro* vs *in vivo* rates of degradation of the particles and release of drug molecules, the independent trafficking globally and at the cellular level in diseased vs healthy tissues, and the behaviors for each of the drug and carrier components, whether intact or in a fragmented form. Clearly, there is much chemistry and biology remaining to be understood, with this work being an important first step for continuing ongoing studies.

■ ASSOCIATED CONTENT

Supporting Information

Experimental details, physical-chemical properties of micelles and SCKs, and confocal microscopy images, including two video files. This material is available free of charge via the Internet at http://pubs.acs.org.

■ AUTHOR INFORMATION

Corresponding Authors

*gustafsontp@icloud.com
*wooley@chem.tamu.edu

Notes

The authors declare no competing financial interest.

■ ACKNOWLEDGMENTS

We thank Dr. Yanwen Yang at The University of Texas MD Anderson Cancer Center, Houston, TX, for his insightful discussion with regard to the CCH-OS-O and SJSA osteosarcoma cell lines. The Welch Foundation is gratefully acknowledged for support through the W. T. Doherty-Welch Chair in Chemistry, Grant No. A-0001. (K.L.W.). D.P.M. Hughes is supported by the NCI of the NIH under award numbers R01CA149501 and R01CA141208. The Microscopy & Imaging Center at Texas A&M University is gratefully acknowledged, and we thank Dr. Hansoo Kim and Dr. Stanislav Vitha for cryo-TEM studies. We thank the VIBS Histology laboratory at the Texas A&M College of Veterinary Medicine, specifically Mrs. Lin Bustamante and Mrs. Chaitali Mukherjee, for their suggestions with regard to the preparation of tissue samples and sections, and the Texas A&M Institute for Genomic Medicine for their expertise and advice in the establishment and breeding of our NSG mouse colony.

■ REFERENCES

(1) Meyers, P. A.; Schwartz, C. L.; Krailo, M. D.; Healey, J. H.; Bernstein, M. L.; Betcher, D.; Ferguson, W. S.; Gebhardt, M. C.; Goorin, A. M.; Harris, M.; Kleinerman, E.; Link, M. P.; Nadel, H.; Nieder, M.; Siegal, G. P.; Weiner, M. A.; Wells, R. J.; Womer, R. B.; Grier, H. E. *J. Clin. Oncol.* **2008**, *26*, 633.
(2) Ottaviani, G.; Jaffe, N. *Cancer Treat. Res.* **2009**, *152*, 3.
(3) Ferguson, W. S.; Goorin, A. M. *Cancer Invest.* **2001**, *19*, 292.
(4) Provisor, A. J.; Ettinger, L. J.; Nachman, J. B.; Krailo, M. D.; Makley, J. T.; Yunis, E. J.; Huvos, A. G.; Betcher, D. L.; Baum, E. S.; Kisker, C. T.; Miser, J. S. *J. Clin. Oncol.* **1997**, *15*, 76.
(5) Bielack, S. S.; Kempf-Bielack, B.; Branscheid, D.; Carrle, D.; Friedel, G.; Helmke, K.; Kevric, M.; Jundt, G.; Kuhne, T.; Maas, R.; Schwarz, R.; Zoubek, A.; Jurgens, H. *J. Clin. Oncol.* **2009**, *27*, 557.
(6) Kempf-Bielack, B.; Bielack, S. S.; Jurgens, H.; Branscheid, D.; Berdel, W. E.; Exner, G. U.; Gobel, U.; Helmke, K.; Jundt, G.; Kabisch, H.; Kevric, M.; Klingebiel, T.; Kotz, R.; Maas, R.; Schwarz, R.; Semik, M.; Treuner, J.; Zoubek, A.; Winkler, K. *J. Clin. Oncol.* **2005**, *23*, 559.

DOI: 10.1021/ja512616s
J. Am. Chem. Soc. 2015, 137, 2056–2066

(7) Hughes, D. P. *Curr. Opin. Oncol.* **2009**, *21*, 332.
(8) Jia, S. F.; Worth, L. L.; Turan, M.; Duan, X. P.; Kleinerman, E. S. *Anti-Cancer Drugs* **2002**, *13*, 155.
(9) Koshkina, N. V.; Kleinerman, E. S.; Waidrep, C.; Jia, S. F.; Worth, L. L.; Gilbert, B. E.; Knight, V. *Clin. Cancer Res.* **2000**, *6*, 2876.
(10) Videira, M.; Almeida, A. J.; Fabra, A. *Nanomedicine* **2012**, *8*, 1208.
(11) Sparreboom, A.; Scripture, C. D.; Trieu, V.; Williams, P. J.; De, T.; Yang, A.; Beals, B.; Figg, W. D.; Hawkins, M.; Desai, N. *Clin. Cancer Res.* **2005**, *11*, 4136.
(12) Gautam, A.; Koshkina, N. *Curr. Cancer Drug Targets* **2003**, *3*, 287.
(13) Singla, A. K.; Garg, A.; Aggarwal, D. *Int. J. Pharmaceutics* **2002**, *235*, 179.
(14) Rowinsky, E. K.; Donehower, R. C. *N. Engl. J. Med.* **1995**, *332*, 1004.
(15) Brannon-Peppas, L.; Blanchette, J. O. *Adv. Drug Delivery Rev.* **2004**, *56*, 1649.
(16) Rowinsky, E. K.; Chaudhry, V.; Cornblath, D. R.; Donehower, R. C. *J. Natl. Cancer Inst. Monogr.* **1993**, 107.
(17) Gelderblom, H.; Verweij, J.; Nooter, K.; Sparreboom, A. *Eur. J. Cancer* **2001**, *37*, 1590.
(18) Wang, J.; Liu, W.; Tu, Q.; Wang, J.; Song, N.; Zhang, Y.; Nie, N.; Wang, J. *Biomacromolecules* **2011**, *12*, 228.
(19) Miele, E.; Spinelli, G. P.; Miele, E.; Tomao, F.; Tomao, S. *Int. J. Nanomed.* **2009**, *4*, 99.
(20) Hamaguchi, T.; Matsumura, Y.; Suzuki, M.; Shimizu, K.; Goda, R.; Nakamura, I.; Nakatomi, I.; Yokoyama, M.; Kataoka, K.; Kakizoe, T. *Br. J. Cancer* **2005**, *92*, 1240.
(21) Wang, A. Z.; Langer, R.; Farokhzad, O. C. *Annu. Rev. Med.* **2012**, *63*, 185.
(22) Kratz, F. *J. Controlled Release* **2008**, *132*, 171.
(23) Green, M. R.; Manikhas, G. M.; Orlov, S.; Afanasyev, B.; Makhson, A. M.; Bhar, P.; Hawkins, M. J. *Ann. Oncol.* **2006**, *17*, 1263.
(24) Ko, Y. J.; Canil, C. M.; Mukherjee, S. D.; Winquist, E.; Elser, C.; Eisen, A.; Reaume, M. N.; Zhang, L. Y.; Sridhar, S. S. *Lancet Oncol.* **2013**, *14*, 769.
(25) Elsabahy, M.; Wooley, K. L. *Chem. Soc. Rev.* **2012**, *41*, 2545.
(26) Zhang, S.; Zou, J.; Elsabahy, M.; Karwa, A.; Li, A.; Moore, D. A.; Dorshow, R. B.; Wooley, K. L. *Chem. Sci.* **2013**, *4*, 2122.
(27) Teow, H. M.; Zhou, Z.; Najlah, M.; Yusof, S. R.; Abbott, N. J.; D'Emanuele, A. *Int. J. Pharmaceutics* **2013**, *441*, 701.
(28) Murphy, E. A.; Majeti, B. K.; Mukthavaram, R.; Acevedo, L. M.; Barnes, L. A.; Cheresh, D. A. *Mol. Cancer Ther.* **2011**, *10*, 972.
(29) Yu, Y.; Chen, C. K.; Law, W. C.; Mok, J.; Zou, J.; Prasad, P. N.; Cheng, C. *Mol. Pharmaceutics* **2013**, *10*, 867.
(30) Liao, L.; Liu, J.; Dreaden, E. C.; Morton, S. W.; Shopsowitz, K. E.; Hammond, P. T.; Johnson, J. A. *J. Am. Chem. Soc.* **2014**, *136*, 5896.
(31) Schmitt-Sody, M.; Strieth, S.; Krasnici, S.; Sauer, B.; Schulze, B.; Teifel, M.; Michaelis, U.; Naujoks, K.; Dellian, M. *Clin. Cancer Res.* **2003**, *9*, 2335.
(32) Liang, K.; Richardson, J. J.; Ejima, H.; Such, G. K.; Cui, J.; Caruso, F. *Adv. Mater.* **2014**, *26*, 2398.
(33) Yu, Y.; Chen, C. K.; Law, W. C.; Weinheimer, E.; Sengupta, S.; Prasad, P. N.; Cheng, C. *Biomacromolecules* **2014**, *15*, 524.
(34) Meng, L.; Huang, W.; Wang, D.; Huang, X.; Zhu, X.; Yan, D. *Biomacromolecules* **2013**, *14*, 2601.
(35) Kataoka, K.; Harada, A.; Nagasaki, Y. *Adv. Drug Delivery Rev.* **2001**, *47*, 113.
(36) Zhang, F.; Elsabahy, M.; Zhang, S.; Lin, L. Y.; Zou, J.; Wooley, K. L. *Nanoscale* **2013**, *5*, 3220.
(37) Matsumura, Y.; Kataoka, K. *Cancer Sci.* **2009**, *100*, 572.
(38) Kato, K.; Chin, K.; Yoshikawa, T.; Yamaguchi, K.; Tsuji, Y.; Esaki, T.; Sakai, K.; Kimura, M.; Hamaguchi, T.; Shimada, Y.; Matsumura, Y.; Ikeda, R. *Invest. New Drugs* **2012**, *30*, 1621.
(39) Emoto, S.; Yamaguchi, H.; Kishikawa, J.; Yamashita, H.; Ishigami, H.; Kitayama, J. *Cancer Sci.* **2012**, *103*, 1304.
(40) Owen, S. C.; Chan, D. P. Y.; Shoichet, M. S. *Nano Today* **2012**, *7*, 53.
(41) Savic, R.; Azzam, T.; Eisenberg, A.; Maysinger, D. *Langmuir* **2006**, *22*, 3570.
(42) Maysinger, D.; Lovric, J.; Eisenberg, A.; Savic, R. *Eur. J. Pharm. Biopharm.* **2007**, *65*, 270.
(43) Lee, N. S.; Lin, L. Y.; Neumann, W. L.; Freskos, J. N.; Karwa, A.; Shieh, J. J.; Dorshow, R. B.; Wooley, K. L. *Small* **2011**, *7*, 1998.
(44) Zhang, S.; Li, Z.; Samarajeewa, S.; Sun, G.; Yang, C.; Wooley, K. L. *J. Am. Chem. Soc.* **2011**, *133*, 11046.
(45) O'Reilly, R. K.; Hawker, C. J.; Wooley, K. L. *Chem. Soc. Rev.* **2006**, *35*, 1068.
(46) Samarajeewa, S.; Shrestha, R.; Elsabahy, M.; Karwa, A.; Li, A.; Zentay, R. P.; Kostelc, J. G.; Dorshow, R. B.; Wooley, K. L. *Mol. Pharmaceutics* **2013**, *10*, 1092.
(47) Tian, H. Y.; Tang, Z. H.; Zhuang, X. L.; Chen, X. S.; Jing, X. B. *Prog. Polym. Sci.* **2012**, *37*, 237.
(48) Huang, S. W.; Wang, J.; Zhang, P. C.; Mao, H. Q.; Zhuo, R. X.; Leong, K. W. *Biomacromolecules* **2004**, *5*, 306.
(49) Wen, J.; Mao, H. Q.; Li, W. P.; Lin, K. Y.; Leong, K. W. *J. Pharm. Sci.* **2004**, *93*, 2142.
(50) Wang, Y. C.; Yuan, Y. Y.; Du, J. Z.; Yang, X. Z.; Wang, J. *Macromol. Biosci.* **2009**, *9*, 1154.
(51) Zhao, Z.; Wang, J.; Mao, H.-Q.; Leong, K. W. *Adv. Drug Delivery Rev.* **2003**, *55*, 483.
(52) Zhang, S.; Zou, J.; Zhang, F.; Elsabahy, M.; Felder, S. E.; Zhu, J.; Pochan, D. J.; Wooley, K. L. *J. Am. Chem. Soc.* **2012**, *134*, 18467.
(53) Sun, C. Y.; Dou, S.; Du, J. Z.; Yang, X. Z.; Li, Y. P.; Wang, J. *Adv. Healthcare Mater.* **2014**, *3*, 261.
(54) Li, A.; Luehmann, H. P.; Sun, G.; Samarajeewa, S.; Zou, J.; Zhang, S.; Zhang, F.; Welch, M. J.; Liu, Y.; Wooley, K. L. *ACS Nano* **2012**, *6*, 8970.
(55) Vila, A.; Gill, H.; McCallion, O.; Alonso, M. J. *J. Controlled Release* **2004**, *98*, 231.
(56) Tang, B. C.; Dawson, M.; Lai, S. K.; Wang, Y. Y.; Suk, J. S.; Yang, M.; Zeitlin, P.; Boyle, M. P.; Fu, J.; Hanes, J. *Proc. Natl. Acad. Sci. U.S.A.* **2009**, *106*, 19268.
(57) Suk, J. S.; Lai, S. K.; Wang, Y. Y.; Ensign, L. M.; Zeitlin, P. L.; Boyle, M. P.; Hanes, J. *Biomaterials* **2009**, *30*, 2591.
(58) Cu, Y.; Saltzman, W. M. *Mol. Pharmaceutics* **2009**, *6*, 173.
(59) Suk, J. S.; Kim, A. J.; Trehan, K.; Schneider, C. S.; Cebotaru, L.; Woodward, O. M.; Boylan, N. J.; Boyle, M. P.; Lai, S. K.; Guggino, W. B.; Hanes, J. *J. Controlled Release* **2014**, *178*, 8.
(60) Shin, H. C.; Alani, A. W. G.; Cho, H.; Bae, Y.; Kolesar, J. M.; Kwon, G. S. *Mol. Pharmaceutics* **2011**, *8*, 1257.
(61) Chen, C. K.; Jones, C. H.; Mistriotis, P.; Yu, Y.; Ma, X.; Ravikrishnan, A.; Jiang, M.; Andreadis, S. T.; Pfeifer, B. A.; Cheng, C. *Biomaterials* **2013**, *34*, 9688.
(62) Deming, T. J. *Nature* **1997**, *390*, 386.
(63) He, X.; Fan, J.; Zhang, F.; Li, R.; Pollack, K. A.; Raymond, J. E.; Zou, J.; Wooley, K. L. *J. Mater. Chem. B* **2014**, *2*, 8123.
(64) Gustafson, T. P.; Lonnecker, A. T.; Heo, G. S.; Zhang, S.; Dove, A. P.; Wooley, K. L. *Biomacromolecules* **2013**, *14*, 3346.
(65) Azechi, M.; Matsumoto, K.; Endo, T. *J. Polym. Sci., Part A: Polym. Chem.* **2013**, *51*, 1651.
(66) Chen, X.; Gross, R. A. *Macromolecules* **1998**, *32*, 308.
(67) Zhai, X.; Huang, W.; Liu, J.; Pang, Y.; Zhu, X.; Zhou, Y.; Yan, D. *Macromol. Biosci.* **2011**, *11*, 1603.
(68) Zou, J.; Zhang, F.; Zhang, S.; Pollack, S. F.; Elsabahy, M.; Fan, J.; Wooley, K. L. *Adv. Healthcare Mater.* **2014**, *3*, 441.
(69) Baran, J.; Penczek, S. *Macromolecules* **1995**, *28*, 5167.
(70) Liu, J.; Huang, W.; Pang, Y.; Zhu, X.; Zhou, Y.; Yan, D. *Biomacromolecules* **2010**, *11*, 1564.
(71) Lu, Z. Z.; Wu, J.; Sun, T. M.; Ji, J.; Yan, L. F.; Wang, J. *Biomaterials* **2008**, *29*, 733.
(72) Elsabahy, M.; Zhang, S.; Zhang, F.; Deng, Z. J.; Lim, Y. H.; Wang, H.; Parsamian, P.; Hammond, P. T.; Wooley, K. L. *Sci. Rep.* **2013**, *3*, 3313.
(73) Yang, X. Z.; Wang, Y. C.; Tang, L. Y.; Xia, H.; Wang, J. *J. Polym. Sci., Part A: Polym. Chem.* **2008**, *46*, 6425.

DOI: 10.1021/ja512616s
J. Am. Chem. Soc. 2015, 137, 2056−2066

(74) Wang, J.; Mao, H. Q.; Leong, K. W. *J. Am. Chem. Soc.* **2001**, *123*, 9480.
(75) Gustafson, T. P.; Lim, Y. H.; Flores, J. A.; Heo, G. S.; Zhang, F.; Zhang, S.; Samarajeewa, S.; Raymond, J. E.; Wooley, K. L. *Langmuir* **2014**, *30*, 631.
(76) Gustafson, T. P.; Cao, Q.; Achilefu, S.; Berezin, M. Y. *ChemPhysChem* **2012**, *13*, 716.
(77) Le Garrec, D.; Gori, S.; Luo, L.; Lessard, D.; Smith, D. C.; Yessine, M. A.; Ranger, M.; Leroux, J. C. *J. Controlled Release* **2004**, *99*, 83.
(78) Choi, H. S.; Ashitate, Y.; Lee, J. H.; Kim, S. H.; Matsui, A.; Insin, N.; Bawendi, M. G.; Semmler-Behnke, M.; Frangioni, J. V.; Tsuda, A. *Nat. Biotechnol.* **2010**, *28*, 1300.
(79) Garbuzenko, O. B.; Mainelis, G.; Taratula, O.; Minko, T. *Cancer Biol. Med.* **2014**, *11*, 44.
(80) Geiser, M.; Kreyling, W. G. *Part. Fibre Toxicol.* **2010**, *7*, 2.
(81) Gonzalez-Angulo, A. M.; Hortobagyi, G. N. *J. Clin. Oncol.* **2008**, *26*, 1585.

DOI: 10.1021/ja512616s
J. Am. Chem. Soc. 2015, 137, 2056−2066